Chemical Engineering Journal 457 (2023) 141335

Contents lists available at ScienceDirect

Chemical Engineering Journal

journal homepage: www.elsevier.com/locate/cej

Reversible multi-electron redox chemistry of organic salt as anode for high-performance Li-ion/dual-ion batteries

Fei Zhang [a], Miaomiao Wu [a], Xingchao Wang [a,*], Qian Xiang [a], Yan Wu [a], Juan Ding [a], Ying Sun [b,*]

[a] State Key Laboratory of Chemistry and Utilization of Carbon Based Energy Resources, College of Chemistry, Xinjiang University, Urumqi 830017, Xinjiang, PR China
[b] Xinjiang Uygur Autonomous Region Product Quality Supervision and Inspection Institute, Key Laboratory of Improvised Explosive Chemicals for State Market Regulation, Urumqi 830011, Xinjiang, PR China

ARTICLE INFO

Keywords:
Organic electrode materials
Multi-electron reaction
Anode
Dual-ion battery
Lithium-ion battery

ABSTRACT

Organic electrode materials are attracting increasing attention for rechargeable secondary batteries because of their low cost, high capacity, nontoxic and environmentally friendly. Herein, we report an excellent anode of a novel organic hexalithium salt of mellitic acid ($Li_6C_{12}O_{12}$) for lithium-ion battery (LIB)/dual-ion battery (DIB). A combination of electrochemical and spectroscopic studies verifies a reversible coordination reaction mechanism based on carboxylic carbonyl and Li^+ ions. $Li_6C_{12}O_{12}$ delivers large reversible capacities of 730 mA h g^{-1} at 0.21 A/g and 372 mA h g^{-1} even at 2 A/g. Furthermore, the $Li_6C_{12}O_{12}$ electrode enables $LiFePO_4$//$Li_6C_{12}O_{12}$ full LIB and graphite//$Li_6C_{12}O_{12}$ full DIB to exhibit high capacity and good cycling stability. This work presents a new perspective on designing and tailoring organic electrode materials to build high-performance lithium-ion batteries/dual-ion batteries.

1. Introduction

Lithium-ion batteries (LIBs) based on graphite anodes have gained great success in powering electric vehicles and portables because of their high capacity and excellent electrochemical reversibility. It is entirely expected that LIBs will completely replace fossil energy as the dominant energy supply of the future [1–12]. However, the current commercialized LIBs can not meet the requirement of high energy density due to the limited capacity of graphite anodes (theoretical capacity ~ 372 mA h g^{-1}) [13–20]. Therefore, developing advanced electrode materials with high electrochemical activity and resource advantages for reviving LIBs is highly desired.

Organic electrode materials are attracting growing attention in recent years due to the advantages of abundant resources, low cost, tunable structure and potentially high capacities [21–26]. In particular, most organic electrode materials are ubiquitous in nature and can be obtained directly or from simple production, which greatly reduces the cost of battery production and is suitable for large-scale applications [27,28]. However, the high dissolution of organic electrodes in aprotic electrolytes causes the server shuttle effect, comprising battery performance, which hinders their application in LIBs [29]. Therefore, various innovative strategies have been developed to solve the problems, such as designing new electrode structures, engineering electrolyte components and modifying the interface of separators [6,21,30–34]. Nevertheless, the strategy is inevitably accompanied by complex manufacturing and an increment in the inactive groups, which significantly increases the cost of batteries and reduces energy density output [35]. Therefore, exploring new anode materials with an exceptional performance through a simple process to enrich LIBs family remains urgent and challenging.

Herein, a new organic carbonyl compound, namely, organic hexalithium salt of mellitic acid ($Li_6C_{12}O_{12}$), was initially introduced as a high-performance anode for Li-storage. $Li_6C_{12}O_{12}$ has a less solubility in the organic electrolytes, thus avoiding the loss of active material during the cycling process. It is demonstrated that $Li_6C_{12}O_{12}$ exhibits a six-electron reaction through the coordination reaction between the carboxylic carbonyl and Li^+ ions. When used as the anode for LIBs, $Li_6C_{12}O_{12}$ shows high reversible capacity (up to 730 mA h g^{-1}) and excellent rate performance (372 mA h g^{-1} at 2 A/g). Two types of $LiFePO_4$//$Li_6C_{12}O_{12}$ full battery and graphite//$Li_6C_{12}O_{12}$ dual-ion battery (DIB) demonstrate outstanding electrochemical performance in terms of high capacity and cycling stability. These excellent authentic

* Corresponding authors.
E-mail addresses: xcwang@xju.edu.cn (X. Wang), ichemabc@126.com (Y. Sun).

https://doi.org/10.1016/j.cej.2023.141335
Received 17 October 2022; Received in revised form 1 December 2022; Accepted 4 January 2023
Available online 5 January 2023

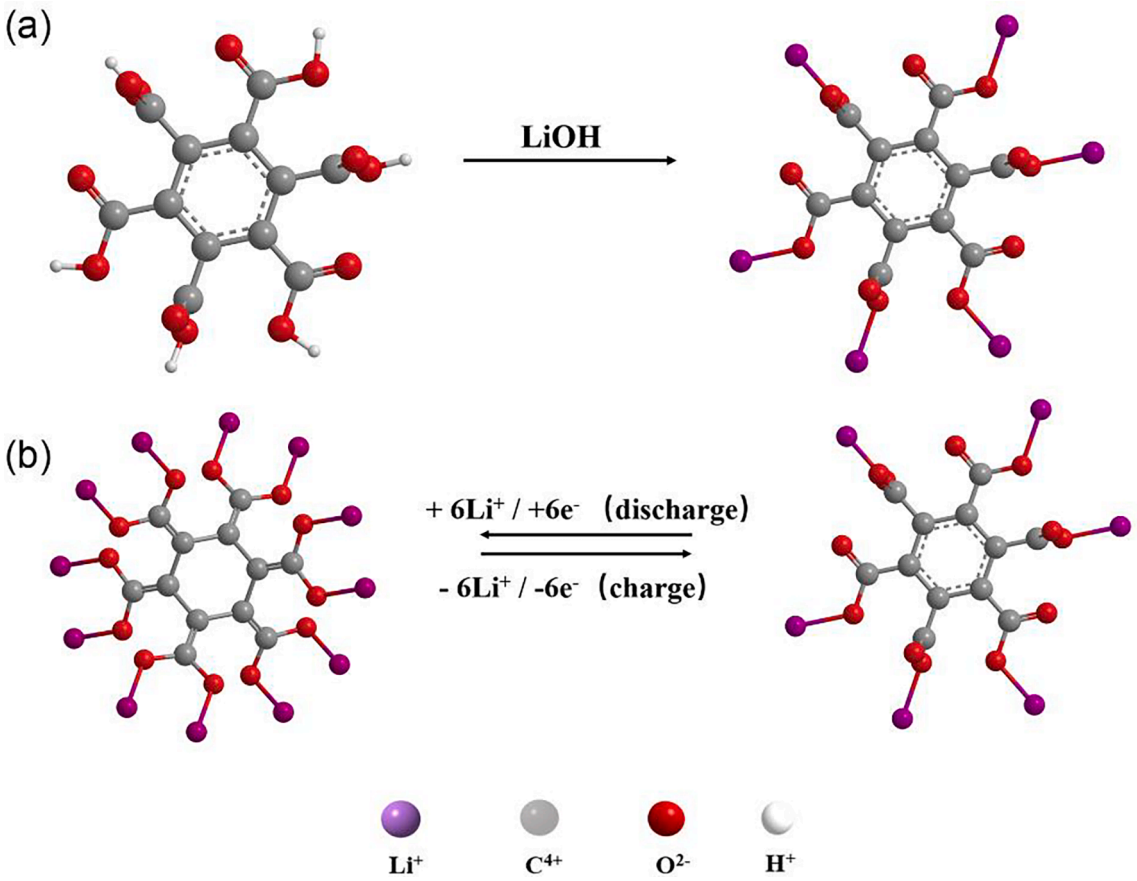

Fig. 1. (a) The scheme of the synthesis process of $Li_6C_{12}O_{12}$ using $H_6C_{12}O_{12}$ and LiOH as raw materials. (b) The storage mechanism of $Li_6C_{12}O_{12}$ electrode for LIBs.

performance are related to the highly reversible reactivity of the carboxyl group and the pseudocapacitive properties of $Li_6C_{12}O_{12}$, as confirmed by comprehensive characterization and theoretical calculations. This work provides a novel strategy for designing organic electrode material with low cost and high performance for LIBs/DIBs.

2. Experimental

2.1. Materials and synthesis

$Li_6C_{12}O_{12}$ was synthesized by a facile precipitation method in an ethanol solution. In a typical procedure, mellitic acid (99 % Sigma-Aldrich) (0.2 g) was firstly dispersed (or dissolved) in ethanol solution (10 mL) to form solution A, and the LiOH (98 % Sigma-Aldrich) (0.1 g) was dissolved in distilled water (10 mL) (denoted as solution B). And then the latter solution was added slowly into solution A under vigorous stirring, and a precipitate was immediately produced. After centrifuging and drying in a vacuum at 180 °C overnight, $Li_6C_{12}O_{12}$ was obtained. The synthesis process is simple and does not require any other high-temperature treatment, making it ideal for mass production.

2.2. Characterization

The morphologies of the sample were examined by SEM HITACHI S4800. FTIR spectra were recorded on a VERTEX 70 from Thermo Scientific. Raman spectra were collected using Bruker SENTERRA II . Raman microscope with 532 nm laser. Hydrogen and carbon NMR were performed using VARIAN INOVA-400 instrument with deuterated chloroform ($CDCl_3$) as solvent. Phase composition transition was confirmed by X-ray diffraction equipment (XRD, Bruker D8 Phaser). Electrochemical impedance spectroscopy (EIS) was collected using a Zanher performed electrochemical workstation at open circuit potential, with constant perturbation amplitude of 5 mV in the frequency of 0.01 Hz−100 KHz.

2.3. Electrochemical measurements

$Li_6C_{12}O_{12}$ (60 %), Ketjen black (30 %) were mixed by a planetary ball mill at a mixing rate of 300 r/min for 2 h. The mixed samples were mixed with poly (vinylidene difluoride) (10 wt%) at the help of *N*-methyl-2-pyrrolidinone, and then cast on Cu foil. The electrodes were dried at 120 °C for 12 h in a vacuum oven, then cut into disks with a diameter of 12 mm. The mass loading of $Li_6C_{12}O_{12}$ was ~ 2 mg cm^{-2}. The electrochemical performance was evaluated by using coin-type (CR2032) cells that were assembled in an argon-filled glovebox (MIKROUNA, Super (1220/750/900)). Li foil and Celgard 2400 were used as counter electrode and separator, respectively. 1 M $LiPF_6$ in an ethylene carbonate-dimethyl carbonate (EC: DEC, by volume, 1: 1) solution was used as electrolyte, and the volume of electrolyte for each cell is 60 μL. Galvanostatic charge/discharge was conducted on a Land CT2001A battery test system in the voltage range of 0.01–3.0 V. Cyclic voltammetric curves were performed using an electrochemical workstation.

2.4. Full cell assembly and tests

To prepare $LiFePO_4$ (LFP) electrode, LFP, Super P and PVDF were mixed in a mortar at a weight ratio of 8.5: 1: 0.5 in 1-Methyl-2-pyrrolidone (NMP), then coated on Al foil and dried under vacuum at 120 °C for 12 h. The full LIBs comprise of LFP as cathode, $Li_6C_{12}O_{12}$ as anode, and 1 M $LiPF_6$ in an ethylene carbonate-dimethyl carbonate solution as electrolyte. To prepare graphite electrode, graphite, Super P and PVDF were mixed with the help of NMP in the weight ratio of 8: 1: 1. The slurry

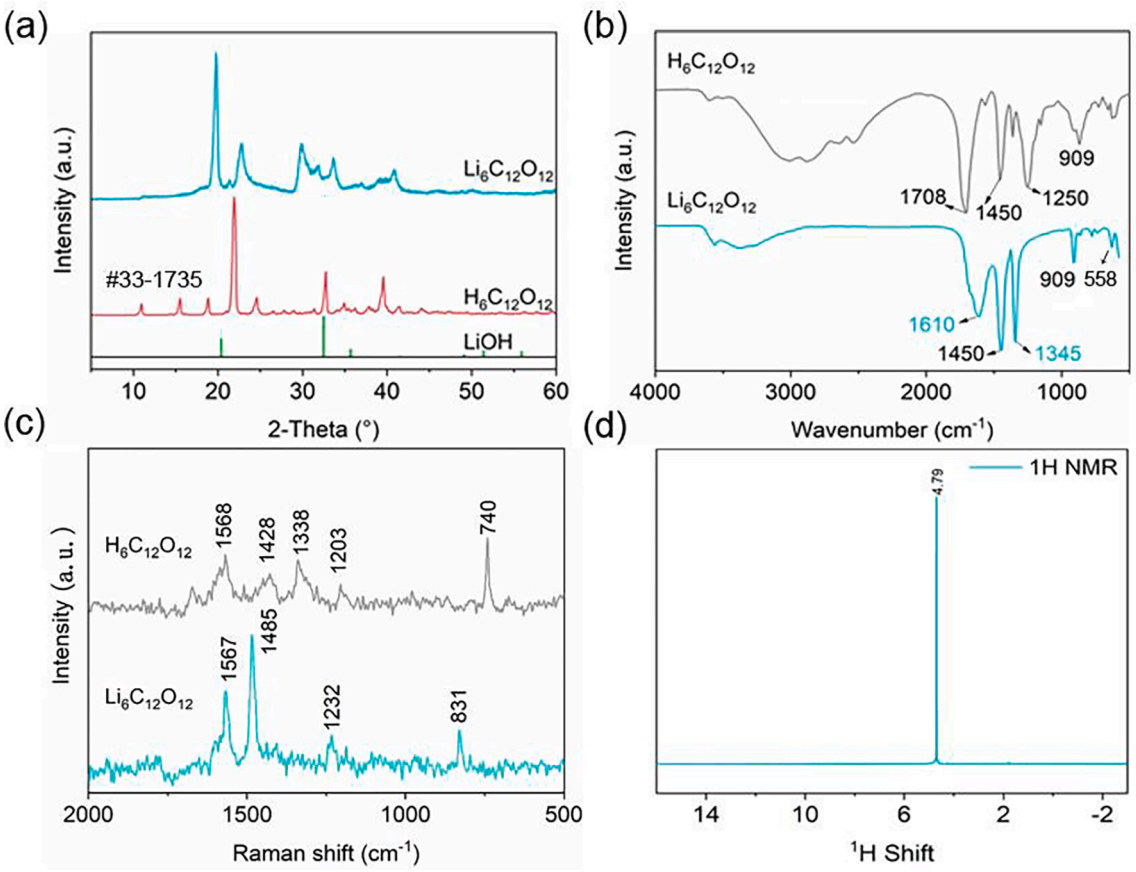

Fig. 2. (a) XRD patterns of $H_6C_{12}O_{12}$, LiOH and $Li_6C_{12}O_{12}$. (b) FT-IR spectrum of $H_6C_{12}O_{12}$ and $Li_6C_{12}O_{12}$. (c) Raman spectrum of $Li_6C_{12}O_{12}$ and $H_6C_{12}O_{12}$. (d) NMR ^{1}H of $Li_6C_{12}O_{12}$.

was evenly coated on Al foil, and then dried in a vacuum even at 110 °C for 12 h. The full DIBs were assembled with graphite as cathode and $Li_6C_{12}O_{12}$ as anode.

2.5. Theoretical calculations

The structural optimization and single-point energy calculations were optimized and calculated by DFT by using the Gaussian 09 package at the B3LYP/6-311G (d) level [36,37]. ESP simulations were performed by Multiwfn software [38], and dynamic visualization processes were simulated by VMD software [39]. Quantitative molecular surface analysis of the ESP is done using Multiwfn, exporting the surface vertex file, loading it into VMD for display, and coloring it according to the B-factor field data (corresponding to the ESP) of vtx. pdb.

3. Results and discussion

Fig. 1a shows the synthesis process and molecular structure of $Li_6C_{12}O_{12}$, which is synthesized via a one-step reaction of $H_6C_{12}O_{12}$ with LiOH in ethanol solution. The synthesis method is simple, green, and suited for scale-up (Fig. S1). $Li_6C_{12}O_{12}$ with six carbonyls is respected to undergo a six-electron reaction and yield a theoretical specific capacity of 450 mA h g^{-1}, which is the notable advantage over graphite anodes (Fig. 1b).

Fig. 2a presents the XRD patterns of the $H_6C_{12}O_{12}$ and LiOH. The characteristic peaks of the resultant $Li_6C_{12}O_{12}$ are quite distinct from those of the $H_6C_{12}O_{12}$ precursor, which tentatively proves the successful synthesis of the material. In addition, NMR, FTIR, and Raman Spectroscopy all confirm the formation of target $Li_6C_{12}O_{12}$ from $H_6C_{12}O_{12}$. Fig. 2b shows the FT-IR spectra of the raw material $H_6C_{12}O_{12}$ and the product $Li_6C_{12}O_{12}$ in the high wavelength range of 3800 to 2000 cm^{-1}. It is clearly found that the absorption peaks of the raw material $H_6C_{12}O_{12}$ are significantly different from those of the product $H_6C_{12}O_{12}$. Specifically, in the FT-IR of $H_{12}C_{12}O_{12}$, the broad absorption peak centered around 3000 cm^{-1} corresponds to the stretching vibration peak of the hydroxyl group (–CO-OH) of $H_6C_{12}O_{12}$. The sharp absorption peak centered at 1708 at 1250 cm^{-1} corresponds to the characteristic absorption peak of the carboxylic acid carbonyl group (-C═O) and the stretching vibration of -C-OH, respectively. By comparison, the characteristic absorption peaks of –CO-OH and -C-OH are not observed in $Li_6C_{12}O_{12}$, while a new peak of lithium-oxygen bond (Li-O) appears at 558 cm^{-1}, due to the complete substitution of H^+ by Li^+ after the reaction of $H_6C_{12}O_{12}$ with LiOH. The peak position of -C═O shifts to 1610 cm^{-1} owing to the strong interaction of Li-O. ^{1}H NMR (Fig. 2d) and ^{13}C NMR (Fig. S2) analyses were performed on the target $Li_6C_{12}O_{12}$. In the ^{13}C NMR spectrum, two resonances at 176.3 and 134.9 ppm were collected, corresponding to the carboxycarbonyl carbon and benzene ring, respectively. The ^{1}H NMR spectrum of $Li_6C_{12}O_{12}$ reveals only one resonance of D_2O at 4.79 ppm and no other proton peaks are observed, strongly proving the successful synthesis of $Li_6C_{12}O_{12}$. Fig. 2c shows the Raman spectra of $H_6C_{12}O_{12}$ and $Li_6C_{12}O_{12}$. It is clearly shown that the sharp peak at 740 cm^{-1} corresponds to the vibration in the O═C-OH plane disappearing after the formation of $Li_6C_{12}O_{12}$ from $H_6C_{12}O_{12}$.

Surface morphologies of $Li_6C_{12}O_{12}$ were investigated by SEM (Fig. 3). It can be seen that $Li_6C_{12}O_{12}$ displays a bulk structure of tens of micrometers in size, which is unfavorable for electron/ion diffusion. Therefore, the bulk $Li_6C_{12}O_{12}$ is mixed with Ketjen black by the ball-mill method to reduce the sizes and improve the conductivity. As expected, the particle size of $Li_6C_{12}O_{12}$ is significantly reduced to 100–200 nm, while the $Li_6C_{12}O_{12}$ particles are tightly wrapped by highly conductive

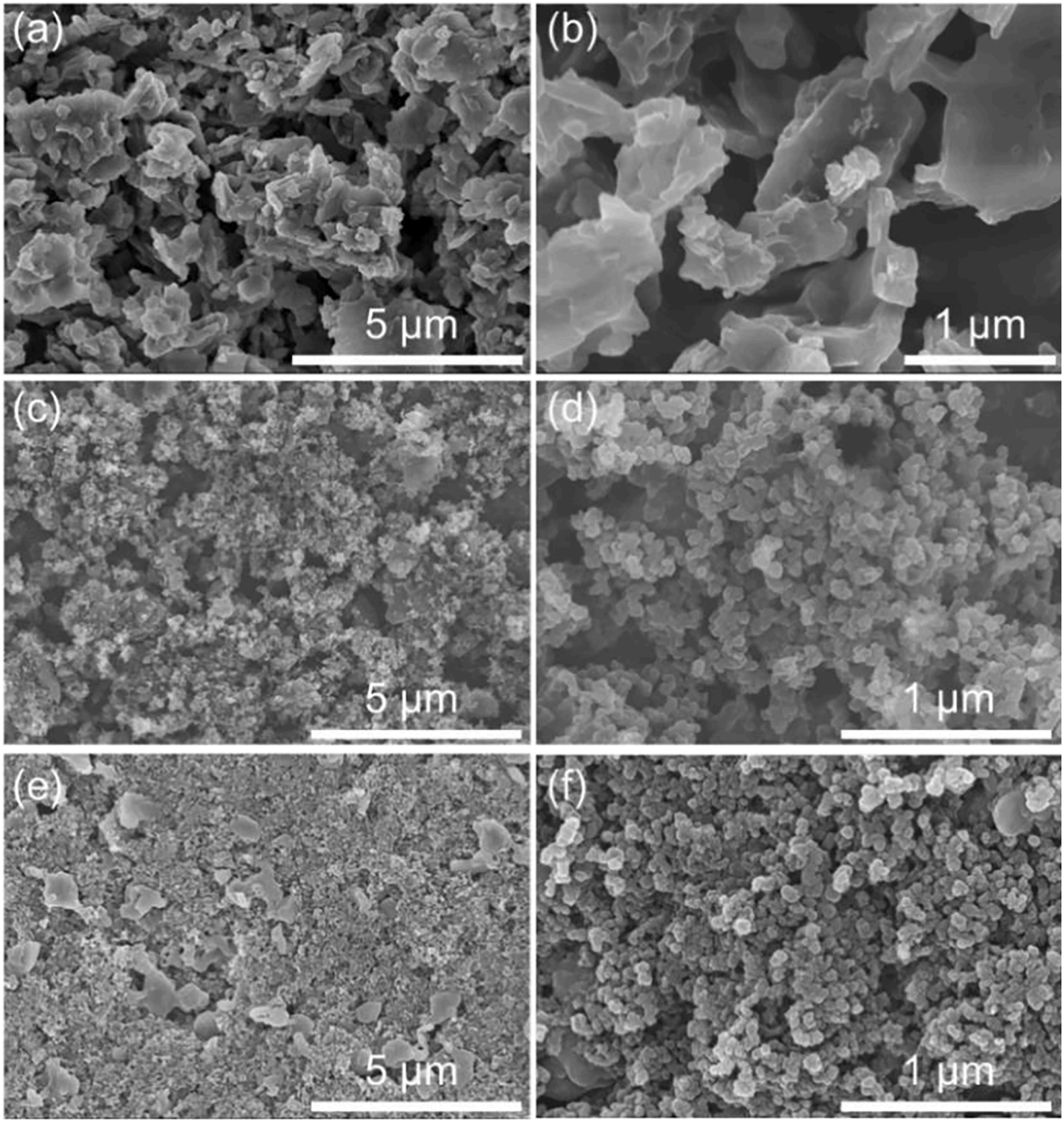

Fig. 3. SEM images of (a-b) $Li_6C_{12}O_{12}$, (c-d) $Li_6C_{12}O_{12}$/KB and (e-f) $Li_6C_{12}O_{12}$ electrode.

carbon, which greatly boosts electron/ion conductivity [40].

The Li-storage behavior of $Li_6C_{12}O_{12}$ electrode was evaluated using a half-cell with a Li anode. Cyclic voltammetry (CV) curves were conducted at a scan rate of 0.1 mV s^{-1} within a voltage of 0.01–3.0 V. In the initial cathodic scan, one couple of distinct redox peaks at 1.25/1.45 V can be observed, corresponding to the insertion/extraction of Li^+ into/from the C═O bonds of COOLi groups (Fig. 4a). The peak at 0.66 V in the first cathodic scan disappears in the subsequent scans due to the formation of SEI film [41]. Remarkably, the CVs are almost overlapped after the first scan, indicative of the excellent reversibility of $Li_6C_{12}O_{12}$. Fig. 4(b) shows the cycling curve of the $Li_6C_{12}O_{12}$ electrode at a current density of 0.21 A/g. The discharge capacity of $Li_6C_{12}O_{12}$ is 527 mA h g^{-1} for the first cycle and reduces to 455 mA h g^{-1} after 10 cycles, which is due to the electrolyte decomposition and partial irreversible reaction of $Li_6C_{12}O_{12}$ electrode. Afterwards, as the electrolyte gradually penetrates and more electrode material is activated, the discharge capacity gradually increases and stabilizes at about 730 mA h g^{-1}. This result is commonly found in anode materials [42]. To investigate the reason for the increase in capacity, AC impedance tests were performed. As shown in Fig. S3, the impedance gradually decreases after fifty turns of the cycle, indicating improved kinetics reaction, which is favorable for fast Li^+/electron transports.

The first discharge and charge capacities of $Li_6C_{12}O_{12}$ are 1719.7 and 527.5 mA h g^{-1}, respectively, corresponding to an initial Coulombic efficiency of 30.8 %. The low Coulombic efficiency of the $Li_6C_{12}O_{12}$ electrode is ascribed to the SEI formation and the irreversible reaction of $Li_6C_{12}O_{12}$. During the following cycles, the reversible capacity first generally decreases and then gradually increases (Fig. 4c). The increase in capacity with cycling may be ascribed to the electrolyte gradually permeating into the $Li_6C_{12}O_{12}$ electrode, which is similar to most

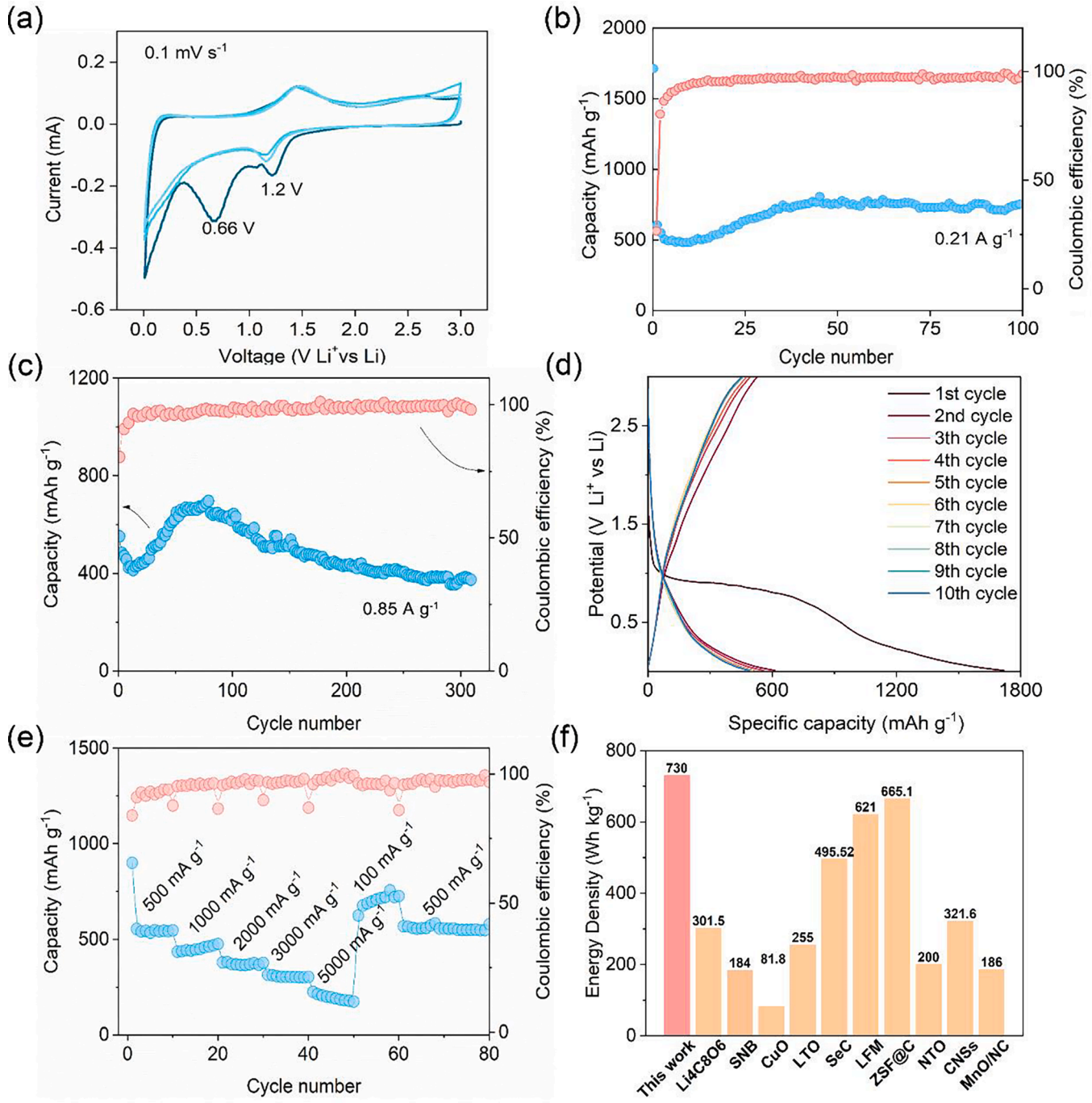

Fig. 4. Electrochemical performance of $Li_6C_{12}O_{12}$ for LIBs. (a) CV curves at 0.1 mV s^{-1}. Cycle performances at the current densities of (b) 0.21 A/g and (c) 0.85 A/g, respectively. (d) Charge/discharge curves after different cycles. (e) Rate performance. (f) Comparison of energy density of $Li_6C_{12}O_{12}$ with other reported anode materials for LIBs.

organic electrode materials [43,44]. Excitingly, a considerable capacity of 374 mA h g^{-1} is obtained even after 300 cycles, (Fig. 4d) shows the charge/discharge curves of $Li_6C_{12}O_{12}$, in which the charge curves and discharge curves are well overlapped after the initial activation cycle, indicating good capacity retention. The rate performance of $Li_6C_{12}O_{12}$ was also investigated at current densities varying from 0.5 to 5 A/g (Fig. 4e). The reversible capacities of $Li_6C_{12}O_{12}$ are 544, 452, 372, 306 and 195 mA h g^{-1} at the current densities of 0.5, 1, 2, 3 and 5 A/g, respectively, suggesting good rate capability. Remarkably, the $Li_6C_{12}O_{12}$ still achieves a stable reversible capacity of 559 mA h g^{-1} when the current density turns back to 0.5 A/g. Such a superior rate performance of $Li_6C_{12}O_{12}$ is mainly ascribed to the fast reactive kinetics and high transport rate of Li^+ ions. Impressively, A remarkable energy density of 730 Wh kg^{-1} was delivered based on the mass of the $Li_6C_{12}O_{12}$ anode, which is superior to most of the recently reported electrode materials in LIBs (Fig. 4f, Table S1).

To further explore the kinetics of electrochemical reactions, CV tests at different scan rates were carried out [45] (Fig. 5a). There are two redox peaks at 1.20 and 1.45 V, which their theoretically calculated b-values were 0.75 and 0.78 (Fig. 5b), respectively, indicating a pseudocapacitive characteristic. The capacitance contribution of $Li_6C_{12}O_{12}$ gradually increases from 46.2 % to 79.0 % as the scan rates increase from 0.1 to 2.0 mV s^{-1} (Fig. 5c, d). Such a pseudocapacitive behavior may be the main reason for exceeding the theoretical capacity.

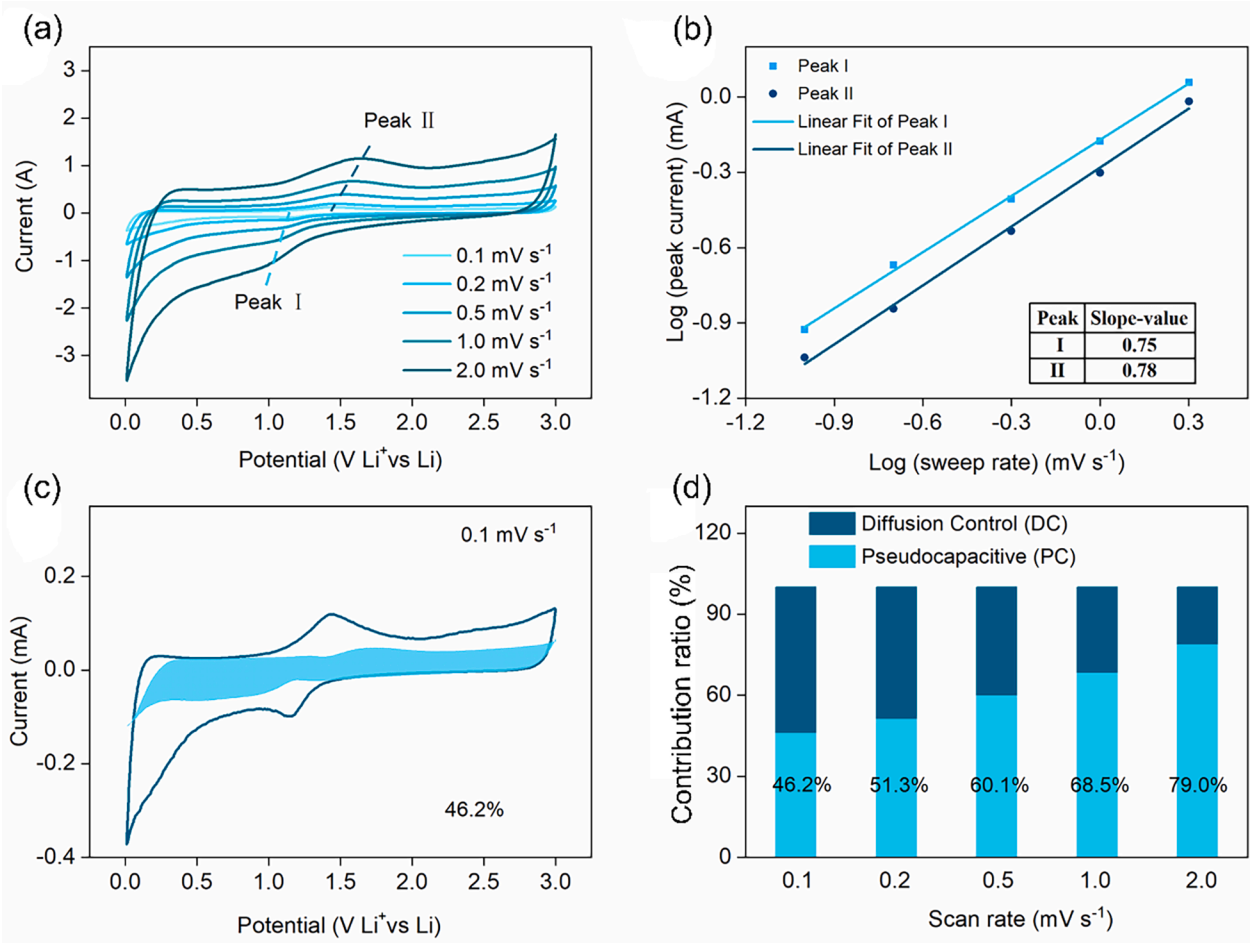

Fig. 5. (a) CV curves of $Li_6C_{12}O_{12}$ at various scan rates. (b) A linear relationship between the peak current and scan rates. (c) Capacitive-controlled contribution at a scan rate of 0.1 mV s^{-1}. (d) Normalized capacitive and diffusion controlled contribution ratios at different scan rates.

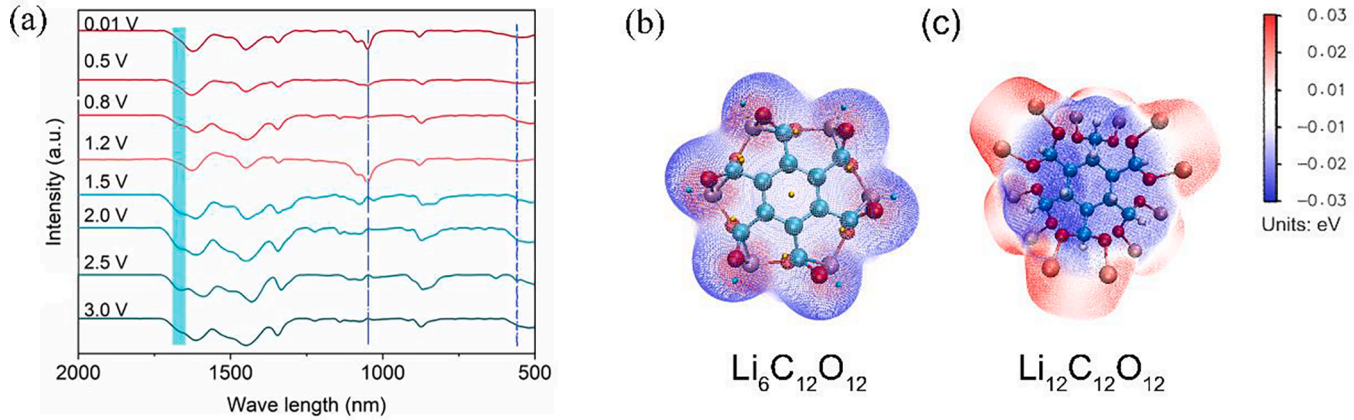

Fig. 6. (a) Ex situ FT-IR of $Li_6C_{12}O_{12}$ electrode at different charge and discharge states. (b) DFT calculations. ESP of (b) $Li_6C_{12}O_{12}$ and (c) $Li_{12}C_{12}O_{12}$.

$$p = a\ v^{b} \quad i\ (1)$$

$$\log(i\ p) = b\ \log(v) + \log(a) \quad (2)$$

$$i\ (V) = k_1\ v + k_2\ v^{1/2} \quad (3)$$

$$i\ (V) / v^{1/2} = k_1\ v^{1/2} + k_2 \quad (4)$$

In the equation, i (V), k_1 v and k_2 $v^{1/2}$ represent the whole current, the pseudocapacitive behavior contribution current, and the diffusion behavior contribution current, respectively. Plotting i (V) / $v^{1/2}$ against $v^{1/2}$, k_1 and k_2 can be found.

To reveal the reversibility and mechanism of the $Li_6C_{12}O_{12}$ electrode, ex-situ FTIR was carried out to observe the molecular vibrations at different charge/discharge states (Fig. 6a). The representative vibration of the -C═O group at about 1700 cm^{-1} gradually vanishes during the discharge process and reappears at the charge states, corresponding to the opening and recovering of C═O of $Li_6C_{12}O_{12}$. Meanwhile, at 1050

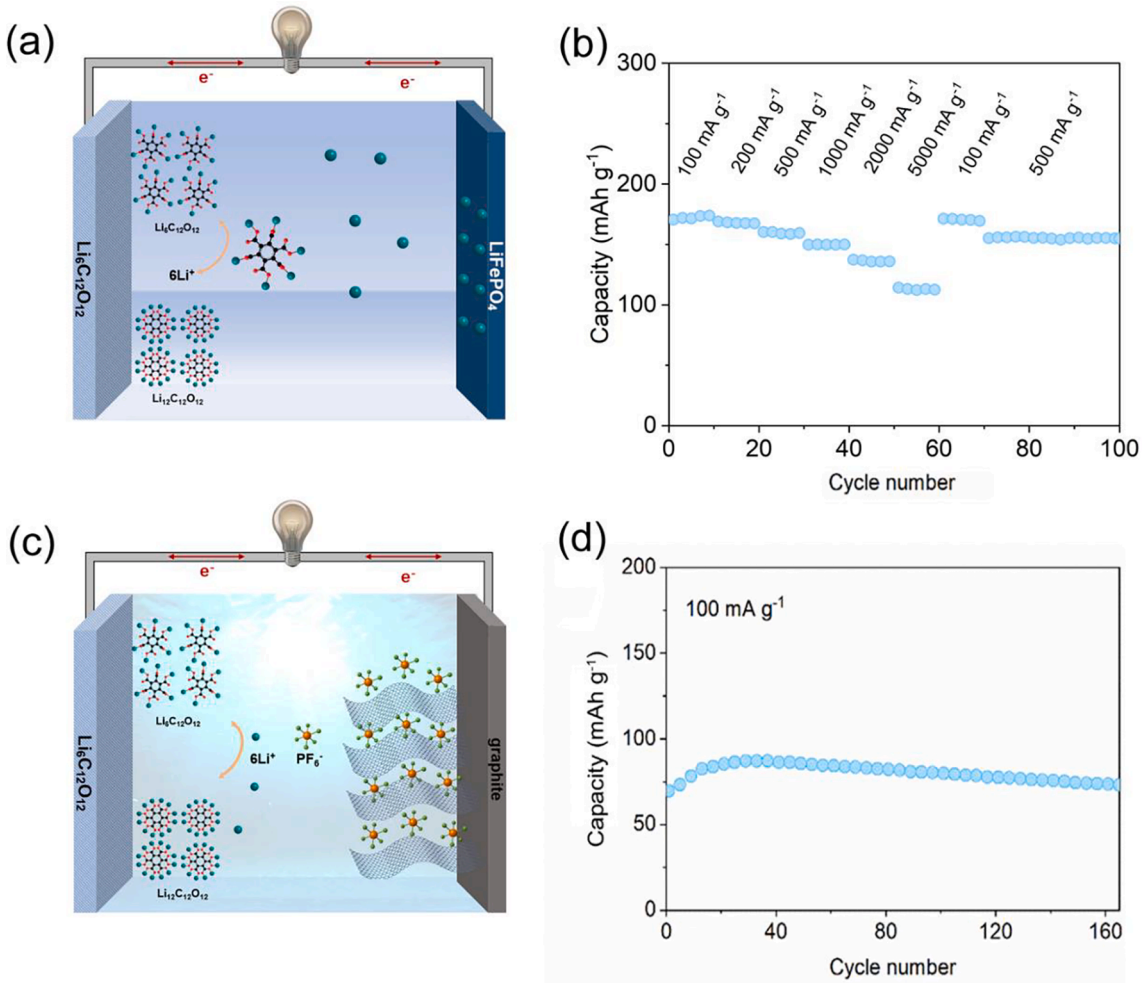

Fig. 7. (a) The scheme and (b) Rate performance of the $LiFePO_4/Li_6C_{12}O_{12}$ full LIB. (c) The scheme and (d) cycle performance of the graphite/$Li_6C_{12}O_{12}$ full LIB.

cm^{-1} corresponds to the stretching vibration of the C—O bond, which gradually disappears during discharge and appears during charging the absorption peak at 558 cm^{-1} gradually disappears upon discharge, while appearing again at charging, which is related to the transition from COO-Li to C═C-$(OLi)_2$, these results indicate the electrochemical reaction based on reversibility of C═O in LTP. The density functional theory calculations (DFT) was performed to investigate the lithiation mechanism of $Li_6C_{12}O_{12}$ [36,37], and the electrostatic potential distributions of $H_6C_{12}O_{12}$ and $Li_{12}C_{12}O_{12}$ were visible in Fig. 6 (b, c). It is clearly observed that the C═O bond of $Li_6C_{12}O_{12}$ shows the lowest electrostatic potential. The blue dot corresponds to the same C═O, which again proves the reaction site. The product $Li_{12}C_{12}O_{12}$ produced an electrostatic potential distribution with a similar symmetric structure after binding to Li^+, substantiating the accuracy of our results [46].

To certify the practical application of the $Li_6C_{12}O_{12}$ electrode in an actual full battery, $LiFePO_4$ (LFP) was used as the cathode to couple with the $Li_6C_{12}O_{12}$ anode to assemble Li-ion full battery. As displayed in Fig. 7 (a, b), the $LiFePO_4//Li_6C_{12}O_{12}$ full battery delivers high capacities (calculated based on the mass of LFP) of 164.9, 161.7, 148.3, 131.4, 110.1 and 76.5 mA h g^{-1} at 17, 34, 85, 170, 340 and 850 mA g^{-1}, respectively. When the rate was turned back to 17 and 85 mA g^{-1}, reversible capacities of 168.5 and 145.2 mA h g^{-1} are still obtained, indicating good rate performance of the full battery.

In addition to the Li-ion full battery, a dual-ion full battery (DIB) employing $Li_6C_{12}O_{12}$ as the anode and graphite as the cathode is also designed in a typical electrolyte (1 M $LiPF_6$ /EC: DEC electrolyte) (Fig. 7c, d). The dual-ion battery can provide high energy density with high output voltage (>4.0 V) while maintaining the advantage of low cost. The cycling performance of the DIB is performed at a current density of 0.1 A/g in the voltage range of 2.5–4.6 V. After 10 cycles of activation, the DIB exhibits a high reversible capacity of ~ 80 mA h g^{-1}, with an energy density of 284 Wh Kg^{-1}. Furthermore, the DIB shows good cycling stability with 91 % capacity retention during 160 cycles. All the results demonstrate the good feasibility of $Li_6C_{12}O_{12}$ as a new anode material for application in DIBs.

4. Conclusion

In summary, we designed a novel organic hexalithium salt $Li_6C_{12}O_{12}$ by a green method at room temperature and investigated its feasibility as a new anode material for LIBs and DIBs. The combination of electrochemical investigations and spectroscopic results demonstrates that $Li_6C_{12}O_{12}$ reveals good reversible Li-storage performance based on the coordination reaction mechanism of the carboxylic carbonyl with Li^+. $Li_6C_{12}O_{12}$ delivers a considerable reversible capacity of 730 mA h g^{-1} and cycling stability at 0.21 A/g. More striking, high capacity, rate performance and cycling stability of $Li_6C_{12}O_{12}//LiFePO_4$ full battery and $Li_6C_{12}O_{12}$//graphite dual-ion battery are also obtained. The superior electrochemical performance of $Li_6C_{12}O_{12}$ is ascribed to the highly reversible reactivity of the carboxyl group and the pseudocapacitive characteristic, as well as less soluble properties in organic electrolytes. This work highlights the active role of designing and tailoring organic electrode materials in building high-performance batteries and capacitors for Li-storage.

Declaration of Competing Interest

The authors declare that they have no known competing financial interests or personal relationships that could have appeared to influence the work reported in this paper.

Data availability

Data will be made available on request.

Acknowledgements

This work was financially supported by the the National Natural Science Foundation of China (22065033, 21905242, U1903217, 21965034 and 21666037), the Natural Science Foundation of Xinjiang Province (2022B01024, 2022D01A105 and 2022D01E35).

Appendix A. Supplementary data

Supplementary data to this article can be found online at https://doi.org/10.1016/j.cej.2023.141335.

References

[1] J. Kim, Y. Kim, J. Yoo, G. Kwon, Y. Ko, K. Kang, Organic batteries for a greener rechargeable world, Nat. Rev. Mater. (2022), https://doi.org/10.1038/s41578-022-00478-1.
[2] J. Wandt, P. Jakes, J. Granwehr, R.-A. Eichel, H.A. Gasteiger, Quantitative and time-resolved detection of lithium plating on graphite anodes in lithium ion batteries, Mater. Today 21 (3) (2018) 231–240, https://doi.org/10.1016/j.mattod.2017.11.001.
[3] A. Huang, Y. Ma, J. Peng, L. Li, S.-L. Chou, S. Ramakrishna, S. Peng, Tailoring the structure of silicon-based materials for lithium-ion batteries via electrospinning technology, eScience 1 (2) (2021) 141–162.
[4] F. Dong, C. Peng, H. Xu, Y. Zheng, H. Yao, J. Yang, S. Zheng, Lithiated sulfur-incorporated, polymeric cathode for durable lithium-sulfur batteries with promoted redox kinetics, ACS Nano 15 (12) (2021) 20287–20299, https://doi.org/10.1021/acsnano.1c08449.
[5] T. Yuan, Z. Tan, C. Ma, J. Yang, Z.-F. Ma, S. Zheng, Challenges of spinel $Li_4ti_5o_{12}$ for lithium-ion battery industrial applications, Adv. Energy Mater. 7 (12) (2017) 1601625, https://doi.org/10.1002/aenm.201601625.
[6] Y. Lu, Y. Cai, Q. Zhang, J. Chen, Insights into redox processes and correlated performance of organic carbonyl electrode materials in rechargeable batteries, Adv. Mater. 34 (22) (2022) 2104150.
[7] T. Jin, X. Ji, P.F. Wang, K. Zhu, J. Zhang, L. Cao, L. Chen, C. Cui, T. Deng, S. Liu, N. Piao, Y. Liu, C. Shen, K. Xie, L. Jiao, C. Wang, High-energy aqueous sodium-ion batteries, Angew. Chem. Int. Ed. 60 (21) (2021) 11943–11948, https://doi.org/10.1002/anie.202017167.
[8] J. Liu, J. Wang, Y. Ni, J. Liu, Y. Zhang, Y. Lu, Z. Yan, K. Zhang, Q. Zhao, F. Cheng, J. Chen, Tuning interphase chemistry to stabilize high-voltage $LiCoO_2$ cathode material via spinel coating, Angew. Chem. Int. Ed. 61 (35) (2022) e202207000.
[9] H. Xu, C. Peng, Y. Yan, F. Dong, H. Sun, J. Yang, S. Zheng, "All-In-One" integrated ultrathin SnS_2@3D multichannel carbon matrix power high-areal–capacity lithium battery anode, Carbon Energy 1 (2) (2019) 276–288, https://doi.org/10.1002/cey2.22.
[10] J. Li, X. Zhao, P. He, Y. Liu, J. Jin, Q. Shen, Y. Wang, S. Li, X. Qu, Y. Liu, L. Jiao, Stabilized multi-electron reactions in a high-energy $Na_4Mn_{0.9}CrMg_{0.1}(PO_4)_3$ sodium-storage cathode enabled by the Pinning Effect, Small 18 (31) (2022) 2202879, https://doi.org/10.1002/smll.202202879.
[11] F. Liu, Y. Liu, X. Zhao, K. Liu, H. Yin, L.Z. Fan, Batteries: Prelithiated V_2C MXene: a high-performance electrode for hybrid magnesium/lithium-ion batteries by ion cointercalation, Small 16 (8) (2020) 2070043, https://doi.org/10.1002/smll.202070043.
[12] J. Liu, Z. Wu, M. Yu, H. Hu, Y. Zhang, K. Zhang, Z. Du, F. Cheng, J. Chen, Building homogenous Li_2TiO_3 coating layer on primary particles to stabilize Li-rich Mn-based cathode materials, Small 18 (10) (2022) e2106337.
[13] Y. Lu, X. Rong, Y.-S. Hu, L. Chen, H. Li, Research and development of advanced battery materials in China, Energy Storage Mater. 23 (2019) 144–153, https://doi.org/10.1016/j.ensm.2019.05.019.
[14] Z. Li, Y. Yang, G. Ding, L. Wei, G. Yao, H. Niu, F. Zheng, Q. Chen, Optimizing the nitrogen configuration in interlayer-expanded carbon materials via sulfur-bridged bonds toward remarkable energy storage performances, J. Mater. Chem. A 10 (18) (2022) 10033–10042, https://doi.org/10.1039/D2TA00608A.
[15] F. Zheng, K. Chu, Y. Yang, Z. Li, L. Wei, Y. Xu, G. Yao, Q. Chen, Optimizing the interlayer spacing of heteroatom-doped carbon nanofibers toward ultrahigh potassium-storage performances, ACS Appl. Mater. Inter. 14 (7) (2022) 9212–9221, https://doi.org/10.1021/acsami.1c24275.
[16] P. Niu, Y. Yang, Z. Li, G. Ding, L. Wei, G. Yao, H. Niu, Y. Min, F. Zheng, Q. Chen, Rational design of a hollow porous structure for enhancing diffusion kinetics of K ions in edge-nitrogen doped carbon nanorods, Nano Res. 15 (9) (2022) 8109–8117, https://doi.org/10.1007/s12274-022-4496-y.
[17] Y. Hu, D. Ye, B. Luo, H. Hu, X. Zhu, S. Wang, L. Li, S. Peng, L. Wang, A binder-free and free-standing cobalt sulfide@carbon nanotube cathode material for aluminum-ion batteries, Adv. Mater. 30 (2) (2018) 1703824, https://doi.org/10.1002/adma.201703824.
[18] L. Li, S. Peng, J.K.Y. Lee, D. Ji, M. Srinivasan, S. Ramakrishna, Electrospun hollow nanofibers for advanced secondary batteries, Nano Energy 39 (2017) 111–139, https://doi.org/10.1016/j.nanoen.2017.06.050.
[19] L. Li, D. Yu, P. Li, H. Huang, D. Xie, C.-C. Lin, F. Hu, H.-Y. Chen, S. Peng, Interfacial electronic coupling of ultrathin transition-metal hydroxide nanosheets with layered MXenes as a new prototype for platinum-like hydrogen evolution, Energy Environ. Sci. 14 (12) (2021) 6419–6427, https://doi.org/10.1039/D1EE02538D.
[20] L. Wang, Y. Hao, L. Deng, F. Hu, S. Zhao, L. Li, S. Peng, Rapid complete reconfiguration induced actual active species for industrial hydrogen evolution reaction, Nat. Commun. 13 (1) (2022) 5785, https://doi.org/10.1038/s41467-022-33590-5.
[21] Z. Zhao-Karger, P. Gao, T. Ebert, S. Klyatskaya, Z. Chen, M. Ruben, M. Fichtner, New organic electrode materials for ultrafast electrochemical energy storage, Adv. Mater. 31 (26) (2019) e1806599.
[22] M. Armand, S. Grugeon, H. Vezin, S. Laruelle, P. Ribiere, P. Poizot, J.M. Tarascon, Conjugated dicarboxylate anodes for Li-ion batteries, Nat. Mater. 8 (2) (2009) 120–125, https://doi.org/10.1038/nmat2372.
[23] C. Peng, G.-H. Ning, J. Su, G. Zhong, W. Tang, B. Tian, C. Su, D. Yu, L. Zu, J. Yang, M.-F. Ng, Y.-S. Hu, Y. Yang, M. Armand, K.P. Loh, Reversible multi-electron redox chemistry of π-conjugated N-containing heteroaromatic molecule-based organic cathodes, Nat. Energy 2 (7) (2017) 17074, https://doi.org/10.1038/nenergy.2017.74.
[24] M. Lee, J. Hong, J. Lopez, Y. Sun, D. Feng, K. Lim, W.C. Chueh, M.F. Toney, Y. Cui, Z. Bao, High-performance sodium–organic battery by realizing four-sodium storage in disodium rhodizonate, Nat. Energy 2 (11) (2017) 861–868, https://doi.org/10.1038/s41560-017-0014-y.
[25] Y. Lu, Q. Zhang, F. Li, J. Chen, Emerging lithiated organic cathode materials for lithium-ion full batteries, Angew. Chem. Int. Ed. (2022) e202216047.
[26] X. Yang, Y. Ni, Y. Lu, Q. Zhang, J. Hou, G. Yang, X. Liu, W. Xie, Z. Yan, Q. Zhao, J. Chen, Designing quinone-based anodes with rapid kinetics for rechargeable proton batteries, Angew. Chem. Int. Ed. 61 (39) (2022) e202209642.
[27] M. Miroshnikov, K. Kato, G. Babu, N.K. Thangavel, K. Mahankali, E. Hohenstein, H. Wang, S. Satapathy, K.P. Divya, H. Asare, P.M. Ajayan, L.M.R. Arava, G. John, Made From Henna! A fast-charging, high-capacity, and recyclable tetrakislawsone cathode material for lithium ion batteries, ACS Sustain. Chem. Eng. 7 (16) (2019) 13836–13844, https://doi.org/10.1021/acssuschemeng.9b01800.
[28] J. Kim, S. Ko, C. Noh, H. Kim, S. Lee, D. Kim, H. Park, G. Kwon, G. Son, J.W. Ko, Y. Jung, D. Lee, C.B. Park, K. Kang, Biological nicotinamide cofactor as a redox-active motif for reversible electrochemical energy storage, Angew. Chem. Int. Ed. Engl. 58 (47) (2019) 16764–16769, https://doi.org/10.1002/anie.201906844.
[29] H. Alt, H. Binder, A. Köhling, G. Sandstede, Investigation into the use of quinone compounds for battery cathodes, Electrochim. Acta 17 (5) (1972) 873–887.
[30] Y. Lu, X. Hou, L. Miao, L. Li, R. Shi, L. Liu, J. Chen, Cyclohexanehexone with ultrahigh capacity as cathode materials for lithium-ion batteries, Angew. Chem. Int. Ed. Engl. 58 (21) (2019) 7020–7024, https://doi.org/10.1002/anie.201902185.
[31] Y. Park, D.S. Shin, S.H. Woo, N.S. Choi, K.H. Shin, S.M. Oh, K.T. Lee, S.Y. Hong, Sodium terephthalate as an organic anode material for sodium ion batteries, Adv. Mater. 24 (26) (2012) 3562–3567, https://doi.org/10.1002/adma.201201205.
[32] Q. Zhao, Z. Zhu, J. Chen, Molecular engineering with organic carbonyl electrode materials for advanced stationary and redox flow rechargeable batteries, Adv. Mater. 29 (48) (2017) 1607007, https://doi.org/10.1002/adma.201607007.
[33] Y. Sun, X. Wang, A. Yang, Y. Huang, W. Jia, D. Jia, F. Cheng, M. Xu, M. Li, Y. Lu, Functional separator with a lightweight carbon-coating for stable, high-capacity organic lithium batteries, Chem. Eng. J. 418 (2021), 129404, https://doi.org/10.1016/j.cej.2021.129404.
[34] X. Wang, Z. Shang, A. Yang, Q. Zhang, F. Cheng, D. Jia, J. Chen, Combining quinone cathode and ionic liquid electrolyte for organic sodium-ion batteries, Chem 5 (2) (2019) 364–375, https://doi.org/10.1016/j.chempr.2018.10.018.
[35] Y. Lu, J. Chen, Prospects of organic electrode materials for practical lithium batteries, Nat. Rev. Chem. 4 (3) (2020) 127–142, https://doi.org/10.1038/s41570-020-0160-9.
[36] M.P.A.P. Uvdal, New scale factors for harmonic vibrational frequencies using the b3lyp density functional method with the triple- basis set 6–311+ g (d, p), J. Phys. Chem. A 109 (2005), https://doi.org/10.1021/jp045733a.
[37] T. Yanai, D.P. Tew, N.C. Handy, A new hybrid exchange–correlation functional using the coulomb-attenuating method (cam-b3lyp), Chem. Phys. Lett. 393 (1–3) (2004) 51–57, https://doi.org/10.1016/j.cplett.2004.06.011.
[38] T. Lu, F. Chen, Multiwfn: a multifunctional wavefunction analyzer, J. Comput. Chem. 33 (5) (2012) 580–592, https://doi.org/10.1002/jcc.22885.
[39] A.D. William Humphrey, K. Schulten, VMD: visual molecular dynamics, J. Mol. Graph icsModell. 14 (1996) 33–38.
[40] C. Wang, D. Du, M. Song, Y. Wang, F. Li, A high-power $Na_3V_2(PO_4)_3$-Bi sodium-ion full battery in a wide temperature range, Adv. Energy Mater. 9 (16) (2019) 1900022, https://doi.org/10.1002/aenm.201900022.
[41] D. Liu, C. Chen, Y. Hu, J. Wu, D. Zheng, Z.-Z. Xie, G. Wang, D. Qu, J. Li, D. Qu, Reduced graphene-oxide/highly ordered mesoporous SiOx hybrid material as an anode material for lithium ion batteries, Electrochim. Acta 273 (2018) 26–33, https://doi.org/10.1016/j.electacta.2018.04.030.

[42] P. Liu, J. Han, K. Zhu, Z. Dong, L. Jiao, Heterostructure $SnSe_2$/ZnSe@PDA nanobox for stable and highly efficient sodium-ion storage, Adv. Energy Mater. 10 (24) (2020) 2000741, https://doi.org/10.1002/aenm.202000741.
[43] S. Wang, L. Wang, K. Zhang, Z. Zhu, Z. Tao, J. Chen, Organic $Li_4C_8H_2O_6$ nanosheets for lithium-ion batteries, Nano Lett. 13 (9) (2013) 4404–4409, https://doi.org/10.1021/nl402239p.
[44] Y. Ding, X. Guo, Y. Qian, L. Zhang, L. Xue, J.B. Goodenough, G. Yu, A liquid-metal-enabled versatile organic alkali-ion battery, Adv. Mater. 31 (11) (2019) e1806956.
[45] C. Choi, D.S. Ashby, D.M. Butts, R.H. DeBlock, Q. Wei, J. Lau, B. Dunn, Achieving high energy density and high power density with pseudocapacitive materials, Nat. Rev. Mater. 5 (1) (2019) 5–19, https://doi.org/10.1038/s41578-019-0142-z.
[46] L. Zhang, H. Wang, X. Zhang, Y. Tang, A review of emerging dual-ion batteries: fundamentals and recent advances, Adv. Funct. Mater. 31 (20) (2021) 2010958, https://doi.org/10.1002/adfm.202010958.